IEEE Access
Multidisciplinary | Rapid Review | Open Access Journal

Received June 10, 2021, accepted July 3, 2021, date of publication July 8, 2021, date of current version July 14, 2021.

Digital Object Identifier 10.1109/ACCESS.2021.3095465

Robust Observer Based on Fixed-Time Sliding Mode Control of Position/Velocity for a T-S Fuzzy MEMS Gyroscope

VAN NAM GIAP[1], HONG-SON VU[2], QUANG DICH NGUYEN[3], AND SHYH-CHOUR HUANG[1], (Senior Member, IEEE)

[1]Department of Mechanical Engineering, National Kaohsiung University of Science and Technology, Kaohsiung 807618, Taiwan
[2]Faculty of Electronics and Electrical Engineering, Hung Yen University of Technology and Education, Hung Yen 160000, Vietnam
[3]Institute for Control Engineering and Automation, Hanoi University of Science and Technology, Hanoi 100000, Vietnam

Corresponding authors: Hong-Son Vu (hongson.ute@gmail.com) and Shyh-Chour Huang (shuang@nkust.edu.tw)

This work was supported in part by the Ministry of Science and Technology of the Republic of China under Contract MOST 110-2221-E-992-062.

ABSTRACT This study focused on a control system of the nonlinear micro-electro-mechanical systems (MEMS) gyroscope. First, sector nonlinearity was used to model a MEMS gyroscope in the Takagi-Sugeno (T-S) fuzzy system. Second, a state observer was designed based on linear matrix inequality (LMI) to identify the optimal eigenvalues of the state tracking error function. Then, full-state fixed-time sliding mode control (FTSMC) was constructed to control the system. Third, a case study of a harmonic disturbance observer was used to address the unknown disturbance of the system. A disturbance observer (DOB) was simply designed based on the error signals of the system outputs and observer outputs. The output signals precisely converged to the predefined trajectories in a very short time, with no overshoots and small of steady-state errors. Moreover, the estimated output states were precisely tracked by the system outputs. These important factors were used to confirm that the control of the T-S fuzzy MEMS was effective and easy to achieve. The study used MATLAB simulation to archive the verification. The maximum of tracking error was $e_4 \in [-4.657 : 5.565] \times 10^{-11}$, and the maximum settling time was $T_{e3} \sim 0.144$ for the error of the $\dot{y}-$ axis and the settling time of the $\dot{x}-$ axis, respectively.

INDEX TERMS Takagi-Sugeno fuzzy system, micro-electro-mechanical systems gyroscope, fixed-time sliding mode control, linear matrix inequality, disturbance observer.

I. INTRODUCTION

In recent years, the development of robotics, artificial intelligence, and automobile devices have resulted in a need for micro-electro-mechanical systems (MEMS) gyroscope need to be used with high-precision requirements. The MEMS gyroscopes can be used to measure the rotation angular velocity due to their size and cost. However, fabrication of a MEMS gyroscope is the main reason for the disturbance sensitivity, parameter variations, and environmental temperature effect inverse problems. To increase the precision of a MEMS gyroscope system, some papers investigated the control methods, such as robust control with active disturbance rejection was proposed for MEMS gyroscope [1]. Robust control with a combination of proportional-derivative and fractional-order sliding mode control (SMC) was designed to control MEMS [2]. An adaptive sliding mode control and fuzzy compensator were introduced for the MEMS gyroscope in [3]. The investigations of neural networks for a MEMS gyroscope can be found in [4]–[7]. Wang *et al.* [8] proposed the control of the z-axis of a MEMS gyroscope by using adaptive fractional-order sliding mode control. Zhang *et al.* [9] investigated SMC with the updating law of a neural network for the MEMS gyroscope. All of these papers achieved good performances for tracking problem of the MEMS gyroscopes. However, disturbance observers for the MEMS gyroscopes have received a minimal attention. In [10] proposed the output feedback control for MEMS gyroscope by using neural network and DOB. Furthermore, the MEMS can be more precise in tracking if its mathematical model can be corrected as a

The associate editor coordinating the review of this manuscript and approving it for publication was Nagarajan Raghavan.

nonlinear model. In [11], [12] the T-S fuzzy model with the linearization modeling method was introduced. To the best of our knowledge, no investigation of the sector nonlinearity method of T-S fuzzy modelling for MEMS gyroscopes has been conducted. Furthermore, a fixed-time sliding mode control and a harmonic disturbance observer also may not be available. These factors are the main motivations of this work. In this work, a system states observer was obtained by LMI with vertical spaces. These estimated states were used to construct sliding mode surfaces. The output tracking errors were used to design a disturbance observer, and a disturbance observer error was exponentially convergent. The mathematical model of the system was represented by the combination of the outer fuzzy membership functions and inner sublinear systems. The system was then called the T-S fuzzy MEMS gyroscope.

The Takagi-Sugeno model was proposed in 1985 [13]. T-S fuzzy modeling of the nonlinear system was investigated in detail as sector nonlinearity and linearization by Tanaka and Wang [14]. The development of T-S fuzzy modeling was described in previous papers [15]–[22]. By using the T-S fuzzy model, the mathematical model of a MEMS gyroscope can be changed into the combination of four fuzzy membership functions and four sublinear systems. Estimating the system states of MEMS can be easier with the linear observer design. After modeling, the disturbance observers can easily apply the requirements of the linear-based model.

Linear matrix inequality (LMI) is well known as the poles placement control method. With any pole of the control system expressed as $\lambda = -a + bi, a > 0$ is required to help the system state remain stable; this can be understood as the control system remaining stable if all its poles are located in the left-half of the complex plane. The eigenvalues are important factors for defining the performance of the control system with the damping, overshoot, settling time, and steady-state [23], [24]. This study used LMI with a vertical boundary to obtain the eigenvalues of the state error function. After estimated states were obtained, a sliding mode for position and velocity control was designed for a MEMS gyroscope system.

Sliding-mode control is the nonlinear control technique that consists of switching and equivalent controls; these control values are used to force the states to converge on the predefined surface and stabilize these states on this surface [25]. Chattering is the main caused of decreased system performance, and it is sourced by the switching control [26]–[30]. This paper applied fixed-time sliding mode control with the aim of obtaining small settling time and small chattering. The basic concept of fixed-time control was introduced in 2012 [31]. Applications of the fixed-time concept can be found in [32]–[36]. To the best of our knowledge, investigations of fixed-time control for a MEMS gyroscope are limited. Furthermore, fixed-time control for the double loops of the position and velocity of the MEMS gyroscope might not be available. This study designed the fixed-time for controlling the position and velocity values of the MEMS gyroscope. Under harsh working condition, the disturbance observer is highly recommended for MEMS gyroscopes.

The disturbance observer is a special case of unknown input estimation, where the disturbance and uncertainty can be suppressed to zero to improve the precision of the control system. In [37], a nonlinear basic disturbance observer (NDOB) was introduced very effectively. The application of a basic disturbance observer was found to achieve synchronization and secure communication in [20] and [22]. The application of NDOB for motor control was described in [38]. The development of NDOB on pendulum system can be found in [39]. Otherwise, some advanced disturbance compensations based on a neural network system were investigated in [6], [40]–[43]. To simplify the procedure of the design of a disturbance observer, this study proposed a new DOB to scope the disturbance and uncertainty of a MEMS gyroscope under the conjunction of an unknown disturbance in exogenous form. The exogenous disturbance observer can be found in previously published papers. An exogenous disturbance observer was proposed for the T-S fuzzy system [44]. The problem of the exogenous inputs of a wind turbine system was investigated [45]. The problem of the exogenous disturbance observer of a robot system was discussed in [46]. In [47], an adaptive DOB was proposed to handle an unknown exogenous disturbance value. In this paper, the disturbance observer was constructed with a high convergence speed. The support of a low-pass filter was presented. These introduced control technique, such as the LMI, the fixed-time sliding mode control, and the disturbance observer, will be introduced to control the MEMS gyroscope system with the motivation of the following published papers. In [48], a new hybrid fractional sliding mode control was introduced to a MEMS gyroscope system. Their paper ignored the disturbance observer. In [9], a neural network was used to compensate for the imprecision of the modeling error of the MEMS system. In [49], the neurodynamic approximation-based quantized control was considered for a MEMS gyroscope subjected to disturbance and uncertainty values. In [50], the disturbance, uncertainty, and chattering could be suppressed by the novel control technique of the state observer-based minimal learning parameter. In [51], the disturbance and uncertainty sigmoid functions were provided to estimate the disturbance. A hysteresis quantizer-based neural estimator to estimate the perturbations of a vehicle was proposed in [52]. The fixed-time of an extended states observer with the function of uncertainty estimation was introduced in [53]. However, the settling time remains high, and there exists overshoot values. Furthermore, among the previously published studies [1]–[9], few investigated disturbance observers. To estimate the disturbance of a MEMS system, a neural network was used to archive the goal [54]. The adaptive neural network with full-states feedback of a MEMS gyroscope was discussed in [55]. In [56], the minimum learning parameter-based neural network was proposed to estimate the perturbations of a MEMS system. The linear extended states observer was used to construct the

lumped disturbance of MEMS system [57]. These mentioned papers that investigated a MEMS gyroscope design have few disturbance observers. Furthermore, the discussions of the exogenous disturbance observer for a MEMS gyroscope are limited. Based on these motivations, this paper proposed a new disturbance observer for a MEMS system. The disturbance is finite convergence. The benefits of finite time were described in [58]–[61]. Furthermore, sector nonlinearity modeling for a MEMS gyroscope was not found. To overcome this limitations, this paper addresses the problem of the DOB based on the FTSMC of the T-S fuzzy MEMS gyroscope. Designing the control for a MEMS gyroscope with the nonlinear characteristics of the springs considered is simple work. However, designing a DOB for a nonlinear MEMS gyroscope is a complicated task. To solve this problem, a nonlinear MEMS gyroscope should be considered as sublinear systems. Furthermore, the fixed-time with the states feedback is good control to reject the chattering problem. Obtaining the mass body velocities of MEMS is a complicated task if physical sensors are used. For these values, estimation by using the states observer is easier but costly work.

The contributions of this study are as follows

1. The MEMS gyroscope model was changed into the format of the T-S fuzzy system with the support of the sector nonlinearity method. Nonlinear springs on the MEMS gyroscope were considered with the nonlinear mathematical model of the MEMS system. The new model of the MEMS gyroscope was built to simplify the control design for the MEMS system. The originality of the control of the new model is as follows: a control with full-states and disturbance observer designs is easier to archive.
2. The system states of the MEMS gyroscope as the x- and y-coordinates and the velocity of the mass body can be precisely estimated by the support of the linear matrix inequality method. These estimated states were used to construct the sliding mode surface for the double loops control of position and velocity. This approach is also a new control technique for the MEMS gyroscope.
3. The fixed-time sliding mode control was designed for controlling the MEMS gyroscope with a simple and effective structure. In the sliding mode design, the estimated state and reference input are used to build the sliding mode surface. Furthermore, the generous disturbance observer is based on the errors of the measured and estimated outputs. The disturbance observer was exponentially convergent with the simple structure.
4. To verify the proposed theory, the Lyapunov candidate was used for theoretical proof. Moreover, MATLAB software was used by simulation that to confirm the proposed theories are good for controlling the MEMS gyroscope and robustness with the disturbance and uncertainty effects.

The novelties of this paper are as follows. The nonlinear springs of the MEMS gyroscope were mentioned. To design the controller for the nonlinear MEMS system, T-S fuzzy modeling was used to reduce the cost of the control and observer designs. The full states were known by the observer with the support of the linear matrix inequality. The positions and velocity controls are perfectly obtained via the feedback of the estimated states. The fixed-time sliding mode control was perfectly designed to obtain the precision tracking values of position and velocity values. The proposed control algorithms are large suggestions of the full-states feedback control, robustness control, and disturbance rejection control. The outline of this paper is as follows. The introduction of the trends of the research topic, method concepts, and contributions of the paper were given in the first section. In the second section, the mathematical modeling of a MEMS gyroscope into the T-S fuzzy system, the preliminary mathematical operation of the fixed-time sliding mode control, linear matrix inequality and the proposed disturbance observer are shown. In section III, the proposed theories for the T-S fuzzy MEMS gyroscope system is shown. In section IV, an illustrative example is given to show the effectiveness and correctness of the proposed methods for a MEMS gyroscope. Finally, the conclusion and future works are given in the last section.

Notes: $A > 0$ and $A < 0$ are the positive and negative matrices, respectively. $I \in R^{m\times m}$ is the identity matrix with $m \times m$ dimension. $s \in R^n, s = [s_1, ... , s_n]^T$ then $sign(s) = [sign(s_1), ... , sign(s_n)]^T$ $sig^{\alpha}(s) = |s|^{\alpha} sig(s)$, and $sign(s) = [\frac{s_1}{|s_1|}, ... , \frac{s_n}{|s_n|}]^T$.

II. MATHEMATICAL MODEL OF A MEMS GYROSCOPE AND PRELIMINARY MATHEMATICS

This section is used to show the mathematical model of a MEMS gyroscope and preliminary mathematical operations. In this study, the complexity of the nonlinear springs of the MEMS gyroscope was shown. Designing a control for the nonlinearity of the MEMS gyroscope is still easy. However, designing the disturbance observer or applying the full-states feedback control is complicated work. To meet these difficult requests, the mathematical model of the MEMS gyroscope should be changed into combinations of the sub-linear systems. Because the T-S fuzzy modeling method consists of combinations of the sub-linear systems and outer fuzzy membership functions, the control design for a nonlinear MEMS gyroscope is equivalent to the design of a controller for the sublinear systems. The mathematical modelling of a MEMS gyroscope is first given as follows:

A. MATHEMATICAL MODELING OF THE MEMS GYROSCOPE

This paper reused the mathematic and parameters of [12]. The MEMS gyroscope model [12] is written as

$$\begin{cases} m\ddot{x} + d_{xx}\dot{x} + (d_{xy} - 2m\Omega_z^*)\dot{y} + (k_{xx} - m\Omega_z^{*2})x + k_{xy}y \\ + k_{x^3}x^3 = u_x^* \\ m\ddot{y} + d_{yy}\dot{y} + (d_{xy} + 2m\Omega_z^*)\dot{x} + (k_{yy} - m\Omega_z^{*2})y + k_{xy}x \\ + k_{y^3}y^3 = u_y^* \end{cases} \quad (1)$$

where x and y are the coordinates of the system. m is mass of the rigid body of the MEMS gyroscope. d_{xx} and d_{yy} are the damping terms. k_{xx} and k_{yy} are the stiffness coefficients for x- and y- axes, respectively. $k_{x^3}x^3$ and $k_{y^3}y^3$ are the stiffness coefficients of the x- and y- axes, respectively. u_x^* and u_y^* are the control signal for the x- and y- axes, respectively. Ω_z^* input is the angular velocity. The MEMS gyroscope can be represented as Figure 1 below.

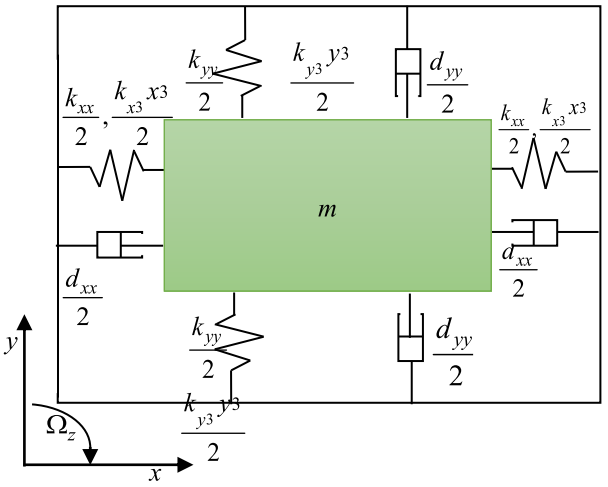

FIGURE 1. **MEMS gyroscope structure.**

Remark 1: In previously published papers, the position controller was introduced to control a MEMS gyroscope. In this work, we proposed the theoretical position and velocity control algorithms.

By dividing both sides of Eq. (1) by the reference mass m, reference length q_0 and resonant frequency Ω_0, the mathematical model of MEMS gyroscope is written as follows:

$$\begin{cases} \dfrac{\ddot{x}}{q_0} + \dfrac{d_{xx}\dot{x}}{m\Omega_0 q_0} + \dfrac{(d_{xy} - 2m\Omega_z^*)\dot{y}}{m\Omega_0 q_0} + \dfrac{(k_{xx} - m\Omega_z^{*2})x}{m\Omega_0^2 q_0} \\ + \dfrac{k_{xy}y}{m\Omega_0^2 q_0} + \dfrac{k_{x^3}x^3}{m\Omega_0^2 q_0} = \dfrac{u_x^*}{m\Omega_0^2 q_0} \\ \dfrac{\ddot{y}}{q_0} + \dfrac{d_{yy}\dot{y}}{m\Omega_0 q_0} + \dfrac{(d_{xy} + 2m\Omega_z^*)\dot{x}}{m\Omega_0 q_0} + \dfrac{(k_{yy} - m\Omega_z^{*2})y}{m\Omega_0^2 q_0} \\ + \dfrac{k_{xy}x}{m\Omega_0^2 q_0} + \dfrac{k_{y^3}y^3}{m\Omega_0^2 q_0} = \dfrac{u_y^*}{m\Omega_0^2 q_0} \end{cases} \tag{2}$$

System (2) can be simplified as follows:

$$\begin{cases} \ddot{x} + a_1\dot{x} + b_1\dot{y} + c_1 x + d_1 y + e_1 x^3 = u_1 \\ \ddot{y} + a_2\dot{y} + b_2\dot{x} + c_2 y + d_2 x + e_2 y^3 = u_2 \end{cases} \tag{3}$$

where the parameter of system (3) can be calculated as $x \to \frac{x}{q_0}, y \to \frac{y}{q_0}, a_1 = \frac{d_{xx}}{m\Omega_0}, b_1 = \frac{(d_{xy}-2m\Omega_z^*)}{m\Omega_0}, c_1 = \frac{(k_{xx}-m\Omega_z^{*2})}{m\Omega_0^2}, d_1 = \frac{k_{xy}}{m\Omega_0^2}, e_1 = \frac{k_{x^3}q_0^2}{m\Omega_0^2}, u_1 = \frac{u_x^*}{m\Omega_0^2 q_0}, a_2 = \frac{d_{yy}}{m\Omega_0}, b_2 = \frac{(d_{xy}+2m\Omega_z^*)}{m\Omega_0}, c_2 = \frac{(k_{yy}-m\Omega_z^{*2})}{m\Omega_0^2}, d_2 = \frac{k_{xy}x}{m\Omega_0^2 q_0}, \frac{k_{y^3}q_0^2}{m\Omega_0^2}$, and $u_2 = \frac{u_y^*}{m\Omega_0^2 q_0}$. The system parameters are as follows: $m = 0.57 \times 10^{-8}$ kg, $\omega_0 = 1$ kHz, $q_0 = 10^{-5}$ m, $\Omega_z = 5$ rad/s, $d_{xx} = 0.429 \times 10^{-6}$ Ns/m, $d_{yy} = 0.429 \times 10^{-6}$ Ns/m, $d_{xy} = 0.429 \times 10^{-6}$ Ns/m, $k_{xx} = 80.98$ N/m, $k_{yy} = 71.62$ N/m, $k_{xy} = 5$ N/m, $k_{x^3} = 3.56 \times 10^6$ N/m, and $k_{y^3} = 3.56 \times 10^6$ N/m. System (3) with full position and velocity control can be modeled as follows:

$$\begin{bmatrix} \dot{x} \\ \dot{y} \\ \ddot{x} \\ \ddot{y} \end{bmatrix} = \begin{bmatrix} 0 & 0 & 1 & 0 \\ 0 & 0 & 0 & 1 \\ -c_1 - e_1x^2 & -d_1 & -a_1 & -b_1 \\ -d_2 & -c_2 - e_2y^2 & -b_2 & -a_2 \end{bmatrix} \begin{bmatrix} x \\ y \\ \dot{x} \\ \dot{y} \end{bmatrix} + \begin{bmatrix} 1 & 0 & 0 & 0 \\ 0 & 1 & 0 & 0 \\ 0 & 0 & 1 & 0 \\ 0 & 0 & 0 & 1 \end{bmatrix} \begin{bmatrix} u_{\dot{x}} \\ u_{\dot{y}} \\ u_1 \\ u_2 \end{bmatrix} \tag{4}$$

where u_1 and u_2 are position control for x- and y-axes, respectively. $u_{\dot{x}}$ is velocity control of x-axis and $u_{\dot{y}}$ is velocity control of the y-axis

Remark 2: In Eq. (4), the velocity control values $u_{\dot{x}}$ for the x-axis and $u_{\dot{y}}$ for the y-axis are added to help improve the precision control of the full-states feedback.

Designing the controller for system (4) is a simple task. However, the number of controllers that can be applied to system (4) may be limited due to its nonlinear format. Furthermore, the DOB design for this nonlinear system is complicated work. To alleviate these control requests, this paper used the sector nonlinearity to convert system (4) into the form of the T-S fuzzy system, which will be called T-S fuzzy MEMS gyroscope system. To represent the sector nonlinearity method, the system

$$\begin{cases} \dot{z} = g^m(z,u)z + h^m(z,u)u \\ y = l^m(z,u)z \end{cases} \tag{5}$$

is considered, where z is a state variable vector. g^m, h^m, and l^m are the smooth functions. y is the output vector. The scheduling variable is $z_j \in [z_{\min}, z_{\max}]$, where $j = 1, .., p$. The weighting functions for z_j are

$$\begin{cases} n_0^j(\cdot) = \dfrac{z_{\max} - z_j(\cdot)}{z_{\max} - z_{\min}} \\ n_1^j(\cdot) = 1 - n_0^j(\cdot) \end{cases} \tag{6}$$

These weighting functions are no longer less than zero. The fuzzy membership function is the product of the weighting functions as follows:

$$\varphi_i(z) = \prod_{j=1}^{p} \varphi_{ij}(z_i) \tag{7}$$

where $\varphi_{ij}(z_i)$ is either $n_0^j(\cdot)$ or $n_1^j(\cdot)$. Because of these concepts, system (5) can be easily modelled as follows:

$$\begin{cases} \dot{z} = \sum_{i=1}^{m} \varphi_i(z)(A_i z + B_i u) \\ y = \sum_{i=1}^{m} \varphi_i(z) C_i z \end{cases} \tag{8}$$

Hence, the system states in (4) are assumed to be $x \in [x_{\max}, x_{\min}]$ and $y \in [y_{\max}, y_{\min}]$, and then, system (4) can be converted into the T-S fuzzy system as follows:

$$\begin{aligned}
&\begin{bmatrix} \dot{x} \\ \dot{y} \\ \ddot{x} \\ \ddot{y} \end{bmatrix} \\
&= \begin{bmatrix} \frac{x^2}{x_{\max}^2} \frac{y^2}{y_{\max}^2} \end{bmatrix} \begin{bmatrix} 0 & 0 & 1 & 0 \\ 0 & 0 & 0 & 1 \\ -c_1 - e_1 x_{\max}^2 & -d_1 & -a_1 & -b_1 \\ -d_2 & -c_2 - e_2 y_{\max}^2 & -b_2 & -a_2 \end{bmatrix} \\
&\quad + (1 - \frac{x^2}{x_{\max}^2}) \frac{y^2}{y_{\max}^2} \begin{bmatrix} 0 & 0 & 1 & 0 \\ 0 & 0 & 0 & 1 \\ -c_1 & -d_1 & -a_1 & -b_1 \\ -d_2 & -c_2 - e_2 y_{\max}^2 & -b_2 & -a_2 \end{bmatrix} \\
&\quad + \frac{x^2}{x_{\max}^2} (1 - \frac{y^2}{y_{\max}^2}) \begin{bmatrix} 0 & 0 & 1 & 0 \\ 0 & 0 & 0 & 1 \\ -c_1 - e_1 x_{\max}^2 & -d_1 & -a_1 & -b_1 \\ -d_2 & -c_2 & -b_2 & -a_2 \end{bmatrix} \\
&\quad + (1 - \frac{x^2}{x_{\max}^2})(1 - \frac{y^2}{y_{\max}^2}) \begin{bmatrix} 0 & 0 & 1 & 0 \\ 0 & 0 & 0 & 1 \\ -c_1 & -d_1 & -a_1 & -b_1 \\ -d_2 & -c_2 & -b_2 & -a_2 \end{bmatrix} \begin{bmatrix} x \\ y \\ \dot{x} \\ \dot{y} \end{bmatrix} \\
&\quad + \begin{bmatrix} 1 & 0 & 0 & 0 \\ 0 & 1 & 0 & 0 \\ 0 & 0 & 1 & 0 \\ 0 & 0 & 0 & 1 \end{bmatrix} \begin{bmatrix} u_{\dot{x}} \\ u_{\dot{y}} \\ u_1 \\ u_2 \end{bmatrix}
\end{aligned} \tag{9}$$

The MEMS gyroscope mathematical model is now calculated as the combination of four fuzzy membership functions and four sublinear systems. To control the MEMS gyroscope in (9), this paper proposed the fixed-time sliding mode control based on the state feedback. To obtain the system states, the LMI is used to obtain the goal. $\hat{x}$ and $\hat{y}$ are used to represent the observer system states. The goal of the sliding mode control is to force these $\hat{x} \to x \to x_r, \hat{y} \to y \to y_r$, $\dot{\hat{x}} \to \dot{x} \to \dot{x}_r, \dot{\hat{y}} \to \dot{y} \to \dot{y}_r$, where r is used to mark the reference term. To this end, the preliminary mathematical operation is presented in the next section.

B. PREMILINARY MATHEMATICS

This section is used to describe the mathematical operations of fixed-time sliding mode control, linear matrix inequality, and exponential convergence disturbance observer. First, to consider the fixed-time concept, the system

$$\dot{x} = f(x, t) \tag{10}$$

where $x(0) = x_0 . x \in R^n$, and $f(x) \in R^n$.

Definition 1: Fixed-time stability [32]

System (10) is called fixed-time stable if the settling time T is globally bounded and $T \leq T_{\max} . T_{\max}$ is a constant value. The system is then called fixed-time stable.

Lemma 1: Consider the equation [32]

$$\dot{s} = -\alpha_1 sig^{\frac{a_1}{b_1}}(s) - \alpha_2 sig^{\frac{a_2}{b_2}}(s) \tag{11}$$

where $\delta(0) = 0, a, b, m, n$ are positively defined. $a_1 > b_1, a_2 < b_2, \alpha_1$, and α_2, are positive values, and the settling time is bounded as follows:

$$T < T_{\max} = \frac{1}{\alpha_1} \frac{b_1}{a_1 - b_1} + \frac{1}{\alpha_2} \frac{b_2}{b_2 - a_2} \tag{12}$$

Proof: The Lyapunov candidate can be chosen with one dimension as follows:

$$V(s) = \frac{1}{2} s s^T \tag{13}$$

Taking derivative of both sides of Eq. (13) yields

$$\begin{aligned}
\dot{V}(s) &= s^T \dot{s} \\
&= s^T (-\alpha_1 sig^{\frac{a_1}{b_1}}(s) - \alpha_2 sig^{\frac{a_2}{b_2}}(s)) \\
&= -\alpha_1 \delta^{2\frac{a_1+b_1}{2b_1}} - \alpha_2 \delta^{2\frac{a_2+b_2}{2b_2}} \\
&= -\alpha_1 V(s)^{\frac{a_1+b_1}{2b_1}} - \alpha_2 V(s)^{\frac{a_2+b_2}{2b_2}} \\
&= [-\alpha_1 V(\delta)^{\frac{a_1+b_1}{2b_1} - \frac{a_2+b_2}{2b_2}} - \alpha_2] V(\delta)^{\frac{a_2+b_2}{2b_2}} \\
&\leq 0
\end{aligned} \tag{14}$$

Because $\dot{V}(s) \leq 0$ system (10) is globally bounded. $V(s) = 0$ is a simple case. $V(\delta) \neq 0$ leads to

$$\frac{1}{V(s)^{\frac{a_2+b_2}{2b_2}}} \frac{dV(s)}{dt} = -\alpha_1 V(s)^{\frac{a1+b_1}{2b_1} - \frac{a_2+b_2}{2b_2}} - \alpha_2 \tag{15}$$

or

$$\begin{aligned}
&\frac{1}{V(s)^{\frac{a_2+b_2}{2b_2}}} \frac{dV(s)}{dt} \\
&= -\alpha_1 V(s)^{\frac{a1+b_1}{2b_1} - \frac{a_2+b_2}{2b_2}} - \alpha_2 \\
&\frac{1}{\alpha_1 V(s)^{\frac{b_2 a_1 - b_1 a_2}{2b_1 b_2}} + \alpha_2} \frac{dV(s)^{\frac{b_2-a_2}{2b_2}}}{dt} = \frac{b_2 - a_2}{b_2}
\end{aligned} \tag{16}$$

Integrating (17) over the time from zero to T yields

$$\int_0^{\infty} \frac{dV(\delta)^{\frac{b_2-a_2}{2b_2}}}{\alpha_1 V(\delta)^{\frac{b_2-a_2}{2b_2}[\frac{(b_2 a_1 - b_1 b_2)}{b_1(b_2-a_2)}+1]} + \alpha_2} = \frac{b_2 - a_2}{2b_2} T \tag{17}$$

or

$$\begin{aligned}
T &< \frac{1}{\frac{b_2-a_2}{b_2}} \int_0^1 \frac{d\varsigma}{\alpha_2} + \frac{1}{\frac{b_2-a_2}{b_2}} \int_1^{\infty} \frac{dV(\delta)^{\frac{b_2-a_2}{2b_2}}}{\alpha_1 V(\delta)^{\frac{(b_2 a_1 - b_1 b_2)}{2b_1 b_2} + \frac{b_2-a_2}{2b_2}}} \\
&= \frac{1}{\alpha_2} \frac{b_2}{b_2 - a_2} + \frac{1}{\alpha_1} \frac{b_2}{b_2 - a_2} \frac{b_1(b_2 - a_2)}{(b_2 a_1 - b_1 b_2)}
\end{aligned} \tag{18}$$

or

$$T_{\max} = \frac{1}{\alpha_2} \frac{b_2}{b_2 - a_2} + \frac{1}{\alpha_1} \frac{b_1}{(a_1 - b_1)} \tag{19}$$

This completes the proof of lemma 1.

Remark 3: For help the reader understand the paper, the proof of the lemma 1 needs to be redone. Lemma 1 is used to illustrate the settling times of each control values in Eq. (55).

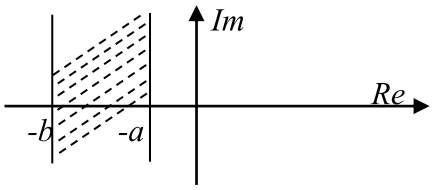

FIGURE 2. Vertical LMI region.

Definition 2: Linear matrix inequality [23]. Consider the system

$$\dot{x}(t) = Ax(t) \tag{20}$$

where $x(t)$ is the system state vector and A is an approximated matrix of $x(t)$. System (20) is called LMI stable if the eigenvalues of the system are located in the region of the LMI condition, and then, there exists a positive matrix P that satisfies

$$A^T P + PA < 0 \tag{21}$$

This paper used the vertical area to find the eigenvalues of the system states errors. The vertical area is referred to as

$$V = \{z \in C : f_V(z) < 0\} \tag{22}$$

where

$$f_V(z) = a + zb + \bar{z}b \tag{23}$$

The V area can be shown as follows:

Lemma 2: For eigenvalues of (20) located in the V area, the eigenvalues of A satisfy $-b < eig(A) < -a$, which can be represented as follows:

$$\begin{cases} A^T P + PA + 2aP < 0 \\ A^T P + PA + 2bP > 0 \end{cases} \tag{24}$$

Proof: The Lyapunov candidates for system (20) are selected as follows:

$$V(x) = x^T P x \tag{25}$$

Taking the derivative of both sides of Eq. (25) yields

$$\begin{aligned} \dot{V}(x) &= \dot{x}^T P x + x^T P \dot{x} \\ &= x^T A^T P x + x^T P A x \\ &= x^T (A^T P + PA) x \end{aligned} \tag{26}$$

$\dot{V}(x) < 0$ and $-b < eig(A) < -a$, if

$$\begin{cases} (A + Ia)^T P + P(A + Ia) < 0 \\ (A + Ib)^T P + P(A + Ib) > 0 \end{cases} \tag{27}$$

or

$$\begin{cases} A^T P + PA + 2aP < 0 \\ A^T P + PA + 2bP > 0 \end{cases} \tag{28}$$

This completes the proof of lemma 2.

Remark 4: Lemma 2 is used to define the observer gains of Eq. (40), where the states observer gains are placed in the LMI region.

The advantages of the LMI with the vertical area are as follows: The LMI with the vertical area is a simple control method that can support the system and obtain the stable eigenvalues in the specific area gap, where the eigenvalues can be archived with the best characteristics of overshoot, damping ratio, and settling time performances.

Definition 3: Disturbance observer-based state observer error.

To show the disturbance observer for this state observer error-based system, the state-space equation is as follows:

$$\begin{cases} \dot{X} = AX + Bu + Dd \\ y = CX \end{cases} \tag{29}$$

where $X \in R^{m\times n}$ is the state vector, $y \in R^{k\times n}$ is the system output vector, $A \in R^{m\times m}$, $B \in R^{m\times p}$, $C \in R^{k\times m}$, and $D \in R^{m\times q}$, are the approximated matrices of states, control input, and perturbations vectors, respectively, and $u \in R^{p\times n}$ is the control input vector. System (29) can work if the disturbance and uncertainty are bounded assumedly as $|d| < \kappa$, where κ is positively defined. The estimated system of (29) can be designed as follows:

$$\begin{cases} \dot{\hat{X}} = A\dot{\hat{X}} + Bu + LC(X - \hat{X}) \\ \hat{y} = C\hat{X} \end{cases} \tag{30}$$

First, consider the case of no disturbance effects on system (29). The state error can be represented as

$$\dot{e} = (A - LC)e \tag{31}$$

By applying the LMI tool box, the observer gain L is found with

$$\begin{cases} (A - LC)^T P + P(A - LC) + 2aP < 0 \\ (A - LC)^T P + P(A - LC) + 2bP > 0 \end{cases} \tag{32}$$

where P, a, b are positively defined. Then, the disturbance observer can be design as follows:

$$\hat{d}(s) = \frac{\gamma}{Ts + \beta^*} Ce(s) \tag{33}$$

or

$$s\hat{d}(s) = -\frac{\beta^*}{T}\hat{d}(s) + \frac{\gamma}{T} Ce(s) \tag{34}$$

By subtracting both sides of (34) by $sd(s)$ yields

$$sd(s) - s\hat{d}(s) = sd(s) + \frac{\beta^*}{T}\hat{d}(s) - \frac{1}{T}\gamma Ce(s) \tag{35}$$

This paper supposes that the source of disturbance can be modeled as

$$\begin{cases} d(t) = v\xi(t) \\ \dot{\xi}(t) = -\omega\xi(t) \end{cases} \tag{36}$$

Eq. (35) can then be modified as follows:

$$\begin{aligned} \dot{\hat{d}}(t) &= -v\omega\xi(t) + v\omega v^{-1}\hat{d}(t) - \frac{\gamma}{T} Ce(t) \\ &= -v\omega v^{-1} d(t) + v\omega v^{-1}\hat{d}(t) - \frac{\gamma}{T} Ce(t) \end{aligned}$$

$$= -v\omega v^{-1}\tilde{d}(t) - \frac{\gamma}{T}Ce(t) \tag{37}$$

where a suitable value of the $v\omega v^{-1} = \frac{\beta^*}{T}$. The disturbance error goes to zero in finite time. This completes the proof of the proposed disturbance observer stability of an exogenous disturbance observer. The details of the applications of these proposed theories to a MEMS gyroscope are shown in the next section.

Remark 5: Definition 3 is used to estimate the perturbation value of the MEMS gyroscope control system in Eq. (43). The low-pass-filter was used to reduce the high-frequency of disturbance value.

III. PROPOSED APPROACH

This section used to show the application of these proposed method on the T-S fuzzy MEMS gyroscope. The structure of this part is as follows: First, states and disturbance observers is designed to the MEMS gyroscope. Second, the fixed-time sliding mode control is designed with full states feedback for controlling the system.

A. STATES AND DISTURBANCE OBSERVER FOR T-S FUZZY MEMS GYROCSOPE

The MEMS gyroscope with full disturbance and uncertainty can be written as follows:

$$\begin{cases} X = \sum_{i,j=1}^{2}(\omega_{ij}(x_i, y_j)[(A_i + \Delta A_i)X \\ \qquad +(B_i + \Delta B_i)u + D_i d]) \\ y = CX \end{cases} \tag{38}$$

with $x_{\max} = 2um$, $y_{\max} = 2um$, $\omega_{11}(x, y) = \frac{x^2}{x_{\max}^2}\frac{y^2}{y_{\max}^2}$, $\omega_{21}(x, y) = (1 - \frac{x^2}{x_{\max}^2})\frac{y^2}{y_{\max}^2}$, $\omega_{12}(x, y) = \frac{x^2}{x_{\max}^2}(1 - \frac{y^2}{y_{\max}^2})$, and $\omega_{22}(x, y) = (1 - \frac{x^2}{x_{\max}^2})(1 - \frac{y^2}{y_{\max}^2})$. System (38) can work if the variation of approximated matrices of the disturbance and uncertainty is bounded as assumption 1 below.

Assumption 1: System (38) can work as its original characteristics if $|\Delta A_i X| < \tau_{i1}, |\Delta B_i u| < \tau_{i2}$, and $|D_i d| < \tau_{i3}$, where $i = 1 \div 2$, all τ_{i1}, τ_{i2}, and τi_3 are positively defined. To easy obtain the information of the disturbance and uncertainty values, these values should be grouped as a unique term of $\Delta A_i X + \Delta B_i u + D_i d = E_i l$.

System (38) can be modified as follows:

$$\begin{cases} \dot{X} = \sum_{i,j=1}^{2} \omega_{ij}(x_i, y_j)[(A_i)X + (B_i)u + E_i l] \\ y = CX \end{cases} \tag{39}$$

Remark 6: Matrix E_i should be identity defined and all these E_i should be identical. The variations of these parameters are unknown.

$$\begin{cases} \dot{\hat{X}} = \sum_{i,j=1}^{2} \omega_{ij}(\hat{x}_i, \hat{y}_j)[(A_i)\hat{X} + (B_i)u + L_{ij}C(X - \hat{X})] \\ y = C\hat{X} \\ \hat{l}(s) = \sum_{i,j=1}^{2} \omega_{ij}(x_i, y_j)[\frac{\delta}{Ts + \varsigma} \\ \qquad \times (E_i^T E_i)^{-1}E_i^T \varepsilon C(X(s) - \hat{X}(s))] \end{cases} \tag{40}$$

Remark 7: The estimated disturbance observer was used to compensate the disturbance of the MEMS gyroscope via the control input channel.

By combining of systems (39) and (40), the tracking error equation can be modeled as follows:

$$\begin{aligned} \dot{e} = &\sum_{i,j=1}^{2} \omega_{ij}(x_i, y_j)[(A_i)X + (B_i)u + E_i(l - \hat{l})] \\ &- \sum_{i,j=1}^{2} \omega_{ij}(\hat{x}_i, \hat{y}_j)[(A_i)\hat{X} + (B_i)u + L_{ij}C(X - \hat{X})] \end{aligned} \tag{41}$$

or

$$\begin{aligned} \dot{e} &= \sum_{i,j=1}^{2} \omega_{ij}(x_i, y_j) \sum_{i,j=1}^{2} \omega_{ij}(\hat{x}_i, \hat{y}_j)[(A_i)X + (B_i)u \\ &\quad + E_i(l - \hat{l}) - (A_i)\hat{X} + (B_i)u + L_{ij}C(X - \hat{X})] \\ &= \sum_{i,j=1}^{2} \omega_{ij}(x_i, y_j) \sum_{i,j=1}^{2} \omega_{ij}(\hat{x}_i, \hat{y}_j)[(A_i - L_{ij}C)e + E_i\tilde{l}] \end{aligned} \tag{42}$$

where L_{ij} is the observer gain and $\tilde{l}$ is the disturbance error. Because, $\sum_{i,j=1}^{2} \omega_{ij}(x_i, y_j) \sum_{i,j=1}^{2} \omega_{ij}(\hat{x}_i, \hat{y}_j)E_i\tilde{l} = E_i\tilde{l}$, the tracking error value can be modified as

$$\dot{e} = \sum_{i,j=1}^{2} \omega_{ij}(x_i, y_j) \sum_{i,j=1}^{2} \omega_{ij}(\hat{x}_i, \hat{y}_j)[(A_i - L_{ij}C)e] + E_i\tilde{l} \tag{43}$$

By applying the LMI to solve the stability of Eq. (43) without disturbance effects, the tracking errors of the measure states and observer converge to each other if

$$\begin{cases} (A_i - L_{ij}C)^T P + P(A_i - L_{ij}C) + 2a_{ij}P < 0 \\ (A_i - L_{ij}C)^T P + P(A_i - L_{ij}C) + 2b_{ij}P > 0 \end{cases} \tag{44}$$

where $b_{ij} < eig(A_i - L_{ij}C) < -a_{ij}$, and P is positively defined. After archiving the precision of the state observer, the disturbance need to be converged to zero, such as $\tilde{l} = 0$, in finite time. By applying the disturbance observer in Eq. (40) to the system (43)

$$\begin{aligned} \dot{e} = &\sum_{i,j=1}^{2} \omega_{ij}(x_i, y_j) \sum_{i,j=1}^{2} \omega_{ij}(\hat{x}_i, \hat{y}_j)[(A_i - L_{ij}C)e] + E_i \\ &\times (l - \sum_{i,j=1}^{2} \omega_{ij}(x_i, y_j)[L^{-1}(\frac{\delta}{Ts + \varsigma}(E_i^T E_i)^{-1}E_i^T \varepsilon Ce(s))] \end{aligned} \tag{45}$$

By combining Eqs. (44), (45) and $\sum_{i,j=1}^{2} \omega_{ij}(x_i, y_j) = 1$, Eq. (45) is archived if

$$l = \hat{l} = L^{-1}(\frac{\delta}{Ts+\varsigma}(E_i^T E_i)^{-1}E_i^T \varepsilon Ce(s)) \tag{46}$$

Taking the Laplace transform of both sides of Eq. (46) leads to

$$\hat{l}(s) = \frac{\delta}{Ts+_{\varsigma}}(E_i^T E_i)^{-1}E_i^T \varepsilon Ce(s) \tag{47}$$

With the exogenous disturbance as Eq. (36), where $l(s) = v\xi(s)$ and $s\xi(s) = -\omega\xi(s)$, system (47) can be changed to

$$(s + \frac{\varsigma}{T})\hat{l}(s) = \frac{1}{T}\delta(E_i^T E_i)^{-1}E_i^T \varepsilon Ce(s) \tag{48}$$

Subtracting both sides of (48) by the $sl(s)$ yields

$$sl(s) - (s + \frac{\varsigma}{T})\hat{l}(s) = sl(s) - \frac{1}{T}\delta(E_i^T E_i)^{-1}E_i^T \varepsilon Ce(s) \tag{49}$$

Eq. (49) can be simplified as follows:

$$\begin{aligned} s\tilde{l}(s) &= sl(s) + \frac{\varsigma}{T}\hat{l}(s) - \frac{1}{T}\delta(E_i^T E_i)^{-1}E_i^T Ce(s) \\ &= -v\omega\xi(s) + \frac{\varsigma}{T}\hat{l}(s) - \frac{1}{T}\delta(E_i^T E_i)^{-1}E_i^T Ce(s) \\ &= -v\omega v^{-1}l(s) + \frac{\varsigma}{T}\hat{l}(s) - \frac{1}{T}\delta(E_i^T E_i)^{-1}E_i^T Ce(s) \\ &= -\rho\tilde{l}(s) - \frac{\varsigma}{T}\delta(E_i^T E_i)^{-1}E_i^T \varepsilon Ce(s) \end{aligned} \tag{50}$$

or

$$\dot{\tilde{l}}(t) = -\rho\tilde{l}(t) - \frac{1}{T}\delta(E_i^T E_i)^{-1}E_i^T \varepsilon Ce(t) \tag{51}$$

With the condition of Eq. (44) and $v\omega v^{-1} \sim \frac{\varsigma}{T} \to \rho$, the disturbance error goes to zero in finite time. This completes the proof of the disturbance observer stability. This study used the estimated states to design the sliding mode control, which is shown in the next section.

B. FIXED-TIME SLIDING MODE CONTROL FOR THE MEMS GYROSCOPE

To archive the fixed time of the reaching phase, the sliding mode surface is proposed as follows:

$$s_i = X_{ri} - \hat{X}_i \tag{52}$$

where $i = 1 \div 4$ is used to represent the element of the states and estimated states. Note that $X_r = \begin{bmatrix} x_r & y_r & \dot{x}_r & \dot{y}_r \end{bmatrix}^T$, $X = \begin{bmatrix} x & y & \dot{x} & \dot{y} \end{bmatrix}^T$ and $\hat{X} = \begin{bmatrix} \hat{x} & \hat{y} & \dot{\hat{x}} & \dot{\hat{y}} \end{bmatrix}^T$.

Differentiating for both sides of Eq. (52) leads to

$$\begin{aligned} \dot{s}_i &= \dot{X}_{ri} - \dot{\hat{X}}_i \\ &= \dot{X}_{ri} - \sum_{i,j=1}^{2} \omega_{ij}(\hat{x}_i, \hat{y}_j)[(A_i)\hat{X}_i + (B_i)u + L_{ij}C(X - \hat{X})] \end{aligned} \tag{53}$$

Since $\sum_{i,j=1}^{2} \omega_{ij}(\hat{x}_i, \hat{y}_j) = 1$, the equivalent control value is

$$u_{eqi} = (B_i^T B_i)^{-1}B_i^T(\dot{X}_{ri} - \sum_{i,j=1}^{2} \omega_{ij}(\hat{x}_i, \hat{y}_j)[(A_i)\hat{X}_i + L_{ij}C(X - \hat{X}))] \tag{54}$$

To archive the fixed time for the reaching phase, the switching control value is proposed as follows:

$$u_{swi} = \eta_i sig^{\frac{p_i}{q_i}}(s) + \chi_i sig^{\frac{m_i}{n_i}}(s) \tag{55}$$

where $i = 1 \div 4$ is used to represent the element of sliding mode surfaces. The control values for velocity controls are

$$u_{\dot{x}} = \dot{X}_{r1} - \sum_{i,j=1}^{2} \omega_{ij}(\hat{x}_i, \hat{y}_j)[(A_{i1})\hat{X} + L_{ij1}C(X - \hat{X})] + \eta_1 sig^{\frac{p_1}{q_1}}(s_1) + \chi_i sig^{\frac{m_1}{n1}}(s_1) \tag{56}$$

for the x-axis, and

$$u_{\dot{y}} = \dot{X}_{r2} - \sum_{i,j=1}^{2} \omega_{ij}(\hat{x}_i, \hat{y}_j)[(A_{i2})\hat{X} + L_{ij2}C(X - \hat{X})] + \eta_2 sig^{\frac{p_2}{q_2}}(s_1) + \chi_2 sig^{\frac{m_2}{n2}}(s_2) \tag{57}$$

for the y-axis. The position controls are

$$u_1 = \dot{X}_{r3} - \sum_{i,j=1}^{2} \omega_{ij}(\hat{x}_i, \hat{y}_j)[(A_{i3})\hat{X} + L_{ij3}C(X - \hat{X})] + \eta_3 sig^{\frac{p_3}{q_3}}(s_3) + \chi_3 sig^{\frac{m_3}{n3}}(s_3) \tag{58}$$

and

$$u_2 = \dot{X}_{r4} - \sum_{i,j=1}^{2} \omega_{ij}(\hat{x}_i, \hat{y}_j)[(A_{i4})\hat{X} + L_{ij4}C(X - \hat{X})] + \eta_4 sig^{\frac{p4}{q4}}(s_4) + \chi_4 sig^{\frac{m4}{n4}}(s_4) \tag{59}$$

for the x- and y-axes, respectively. $A_{i1}, A_{i2}, A_{i3}, A_{i4}$ are rows 1 to 4 of matrix A_i.L_{ij1}, $L_{ij2}, L_{ij3}, L_{ij4}$, *are* rows 1 to 4 of matrix L_{ij}.

C. STABILITY OF THE PROPOSED METHODS

To theoretically verify that the proposed methods are correct, the Lyapunov candidate is assumed as follows:

$$V(s) = \frac{1}{2}s^T s \tag{60}$$

Differentiating of both sides of Eq. (56) yields

$$\begin{aligned} \dot{V}(s) &= s^T \dot{s} \\ &= s^T(\dot{X}_r - \sum_{i,j=1}^{2} \omega_{ij}(\hat{x}_i, \hat{y}_j)[(A_i)\hat{X} + (B_i)u \\ &\quad + L_{ij}C(X - \hat{X})]) \end{aligned} \tag{61}$$

Combining Eqs. (54), (59), and (61) leads to

$$\dot{V}(s_i) = -s_i^T(\eta_i sig^{\frac{p_i}{q_i}}(s_i) + \chi_h sig^{\frac{m_i}{m_i}}(s_i)) < 0 \quad (62)$$

By using lemma 1 for Eq. (58), the settling time for the reaching phase is then the fixed-time stability. The general settling time can be represented as follows:

$$T_i < T_{\max i} = \frac{1}{\eta_i}\frac{q_i}{p_i - q_i} + \frac{1}{\chi_i}\frac{n_i}{n_i - m_i} \quad (63)$$

The illustration of the proposed methods by MATLAB simulation is given in the next section.

Remark 8: The control parameters selection is the main factor effecting the control output performances. This paper has procedures for parameter selection, as LMI gains should be used to obtain small overshoots, damped, small settling times. The source of chattering and overshoot of sliding-mode control is switching control gain. Therefore, the fixed-time sliding mode control gain should be suitably chosen to obtain small settling times, small chattering. The high disturbance observer gains will occur the high oscillation but a fast response, while small gains lead to a slower the disturbance response.

The details of the proposed control algorithms for the MEMS gyroscope are represented in the below diagram.

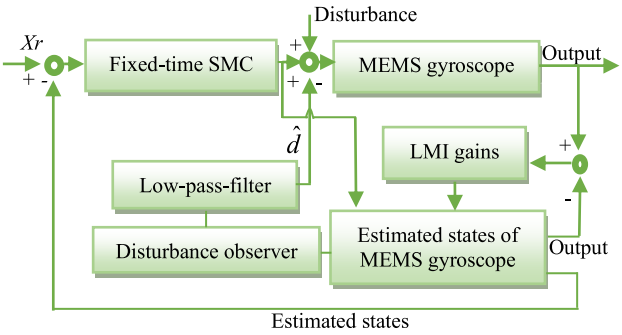

FIGURE 3. Diagram of the proposed algorithms for MEMS gyroscope.

IV. AN ILLUSTRATIVE EXAMPLE

Through the simulation sign $\wedge$ is replace by the word "hat". The simulation performances of the proposed method, named the disturbance observer based on fixed-time sliding mode control for the T-S fuzzy MEMS gyroscope is shown in this section. With the system parameters as Eq. (38), where

$$B_1 = B_2 = B_3 = B_4 = \begin{bmatrix} 1 & 0 & 0 & 0 \\ 0 & 1 & 0 & 0 \\ 0 & 0 & 1 & 0 \\ 0 & 0 & 0 & 1 \end{bmatrix} C = \begin{bmatrix} 1 & 0 & 0 & 0 \\ 0 & 1 & 0 & 0 \end{bmatrix},$$

$$L_{11} = \begin{bmatrix} -0.0300 & -0.0000 \\ -0.0000 & -0.0300 \\ 7.1061 & 0.4386 \\ 0.4386 & 6.2851 \end{bmatrix}.10^3,$$

$$L_{12} = \begin{bmatrix} -0.0200 & -0.0000 \\ -0.0000 & -0.0200 \\ 7.1030 & 0.4386 \\ 0.4386 & 6.2851 \end{bmatrix}.10^3,$$

$$L_{21} = \begin{bmatrix} -0.0125 & -0.0000 \\ -0.0000 & -0.0125 \\ 7.1061 & 0.4386 \\ 0.4386 & 6.2820 \end{bmatrix}.10^3,$$

$$L_{22} = \begin{bmatrix} -0.0160 & -0.0000 \\ -0.0000 & -0.0160 \\ 7.1030 & 0.4386 \\ 0.4386 & 6.2820 \end{bmatrix}.10^3.$$

the LMI condition parameter are as follows:

$a_{11} = 10, b_{11} = 50, a_{12} = 10, b_{12} = 30, a_{12} = 5, b_{12} = 20, a_{22} = 2$, and $b_{22} = 30$. The eigenvalues of measured and estimated states are as follows: $eig(A_1 - L_{11}C)$ are $-15.0350 + 84.1035i$, $-15.0350 - 84.1035i$, $-15.0064 + 76.6228i$, and $-15.0064 - 76.6228i$. $eig(A_2 - L_{12}C)$ are $-10.0350 + 84.8258i$, $-10.0350 - 84.8258i$, $-10.0064 + 77.4305i$, and $-10.0064 - 77.4305i$. $eig(A_3 - L_{21}C)$ are $-6.2850 + 85.1953i$, $-6.2850 - 85.1953i$, $-6.2564 + 77.8090i$, and $-6.2564 - 77.8090i$. $eig(A_4 - L_{21}C)$ are $-8.0350 + 85.0340i$, $-8.0350 - 85.0340i$, $-8.0064 + 77.6456i$, and $-8.0064 - 77.6456i$. These parameters are used for two cases of study. In both cases, the fixed-time control gains and disturbance control gains are tuning. The details are shown below.

Case 1:

The disturbance observer gains are selected as follows: $T = 0.00001$, $\varsigma = 1, \varepsilon = 1000$, and $\delta = 100$. By referring $s_1 = x_r - \hat{x}, s_2 = y_r - \hat{y}, s_3 = \dot{x}_r - \dot{\hat{x}}$, and $s_4 = \dot{y}_r - \dot{\hat{y}}$ are the sliding surfaces of the state and the velocity of the MEMS rigid body. The initial conditions are $X(0) = \hat{X}(0) = [0.005, 0.015, 0, 0]^T$. The fixed-time parameters are as follows: $\eta_1 = 10, \chi_1 = 5, p_1 = 3, q_1 = 4, m_1 = 7, n_1 = 4, \eta_2 = 3, \chi_2 = 2, p_2 = 4, q_2 = 5, m_2 = 7, n_2 = 5, \eta_3 = 20, \chi_3 = 15, p_3 = 3, q_3 = 4, m_3 = 5, n_3 = 4, \eta_4 = 30, \chi_4 = 20, p_4 = 7, q_4 = 8, m_4 = 3$, and $n_4 = 2$. The performances of the proposed control theories on a MEMS gyroscope are shown as the figures below.

These estimated outputs are good at tracking the measured outputs. The impression of the tracking values are shown in Figure 6.

The settling times on the position of the x-axis and y-axis are $T_{e1} \sim 0.1056$ seconds and $T_{e2} \sim 0.09$ seconds, respectively. The settling times on the velocity of the x-axis and y-axis are $T_{e3} \sim 0.144$ seconds and $T_{e4} \sim 0$ second, respectively. The steady-states of the position on x-axis and y-axis are $e_1 \in [-5.618 : 5.619] \times 10^{-12}$ m and $e_2 \in [-4.358 : 4.358] \times 10^{-12}$m, respectively. The steady state of the velocity on the x-axis and y-axis are $e_3 \in [-4.657 : 5.656] \times 10^{-11}$ m and $e_4 \in [-2.238 : 2.236] \times 10^{-12}$(m), respectively. The steady states are quite small. The estimated and measured outputs are quite similar to each other. In [3],

an adaptive SMS and fuzzy compensator were introduced to a MEMS gyroscope; the settling was given as approximately 0.2 second, and the magnitude scale of the tracking error was 10^{-3}. With the high-magnitudes tracking error values, the energy consumption values of the position controls in [3] are smaller than those of our paper. However, our paper can obtain better control factors as small as of those of steady states and settling times. In [5], the results are intuitively larger than our obtained results. In [5], the adaptive neural backstepping PID global SMC was introduced to a MEMS with high-oscillation control input, while the control input for the position control values of this paper is smooth, as shown Figure 8a. Their paper showed that the simple controller consumed less energy. Thus, the energy consumptions values are mostly smaller and smoother than that of [5]. Otherwise, the comparison of this study with the earlier studies [5] is shown in the table below.

Values	OUR PAPER RESULT	PAPER [5]
* *Overshoot*	On a scale 10^{-12} for the x-axis and 10^{-12} for the y-axis	Overshoots area approximated to be 0.4 and 0.25 seconds for the x-axis and the y-axis, respectively
* *Settling time*	$T_{e1} \sim 0.1056$ s $T_{e2} \sim 0.09$ s	After 1 (second)
* *States errors*	$e_1 \in [-5.618 : 5.619] \times 10^{-12}$ m $e_2 \in [-4.358 : 4.358] \times 10^{-12}$ m	Did not clearly show results but more unstable than our outcome
* *Background*	Simulation	Simulation

The performance of the disturbance is shown in Figure 7 below.

The functions of $d_x = \sin(2\pi t)$ and $d_y = 1.5\sin(2.75\pi t)$ were tested on the x- and y- axes of the MEMS system, respectively. To completely reject the disturbances on the x-axis and y-axes is difficult for a nonlinear MEMS gyroscope. In this paper, the tested disturbances were mostly deleted by the estimated disturbances compensation. The control inputs are shown in Figure 8.

The position control was precisely archived by the good position tracking error values on x-, and y-axes. Beyond that point, the inner velocity control input signals are very small compared with the control inputs of the position control. This result shows that the proposed disturbance observer has a strong effect on the unknown exogenous disturbances value, and the proposed fixed-time control method is effective with the T-S fuzzy MEMS gyroscope system. In Figure 8 (b), the control system of MEMS gyroscope exhibits chattering. However, using double loops of position and velocity controls obtains smooth position tracking responses on the x- and y-axes, respectively. The chattering in this paper is very small by using suitable fixed-time control gains.

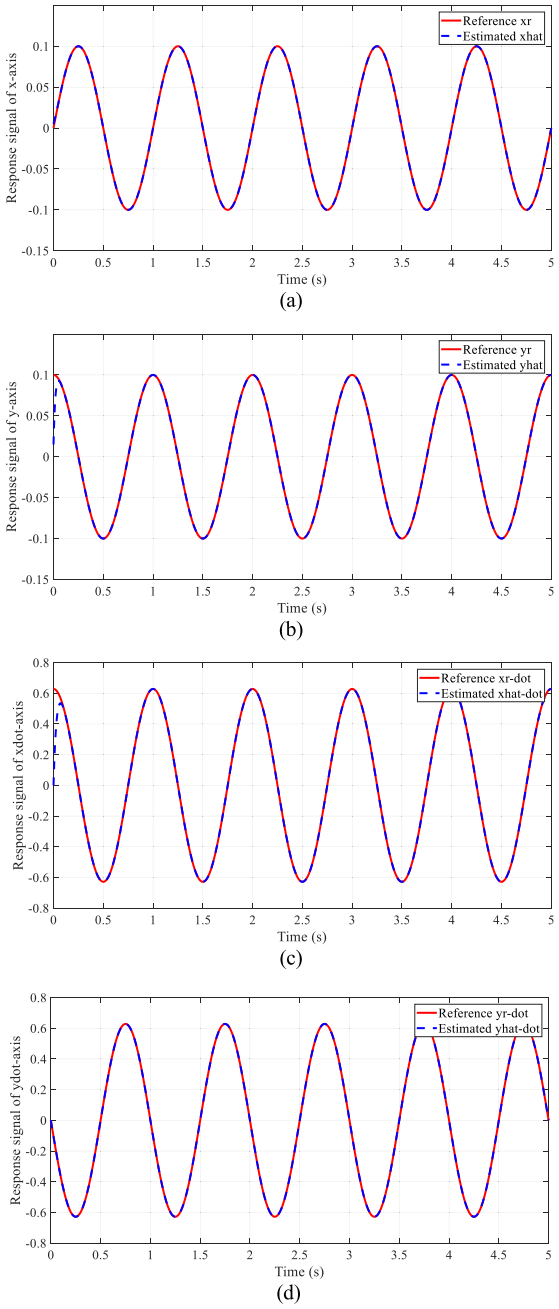

FIGURE 4. Referenced and estimated states: (a) states on the *x*-axis, (b) states on the *y*-axis, (c) states on the *x-dot*-axis, and (d) states on the *y-dot*-axis.

Case 2:

To obtain better control outputs of MEMS gyroscope control system, the parameters are tuned with suitable of the MATLAB-based hardware system as digital signal processor (DSP), field-programmable gate array (FPGA) device. The detail of experiment setup can be found in [62]. Some parameters of the controller and disturbance observer are tuning as $T = 0.00001$, $\varsigma = 1$, $\delta = 100$, and $\varepsilon = 10000$. The initial conditions are $X(0) = \hat{X}(0) = [0.05,\ 0.15,\ 0,\ 0]^T$. The fixed-time parameters are as follows: $\eta_1 = 10$, $\chi_1 = 5$, $p_1 = 3$, $q_1 = 4$, $m_1 = 7$, $n_1 = 4$, $\eta_2 = 3$, $\chi_2 = 2$, $p_2 = 4$, $q_2 = 5$,

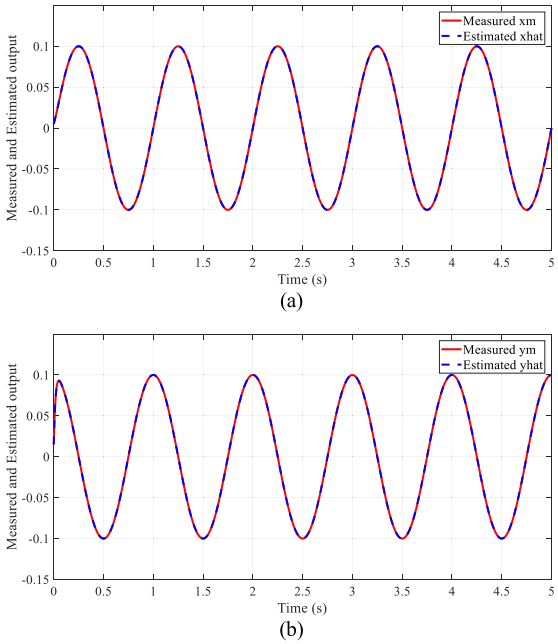

FIGURE 5. Measured and estimated states: (a) states on the *x*-axis and (b) states on the *y*-axis.

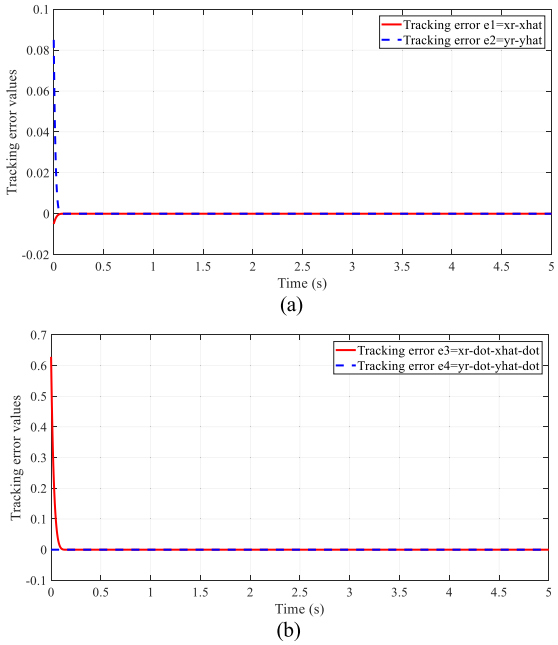

FIGURE 6. Tracking errors of position (a) and velocity (b).

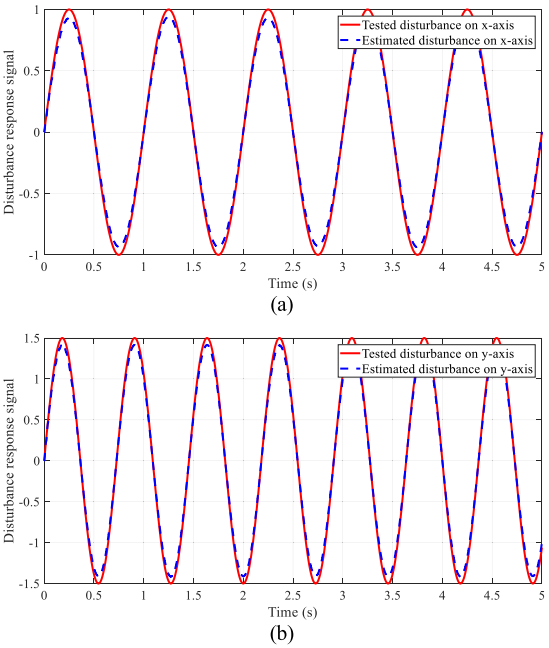

FIGURE 7. Tested and estimated disturbances on *x*- (a) and *y*-axes (b).

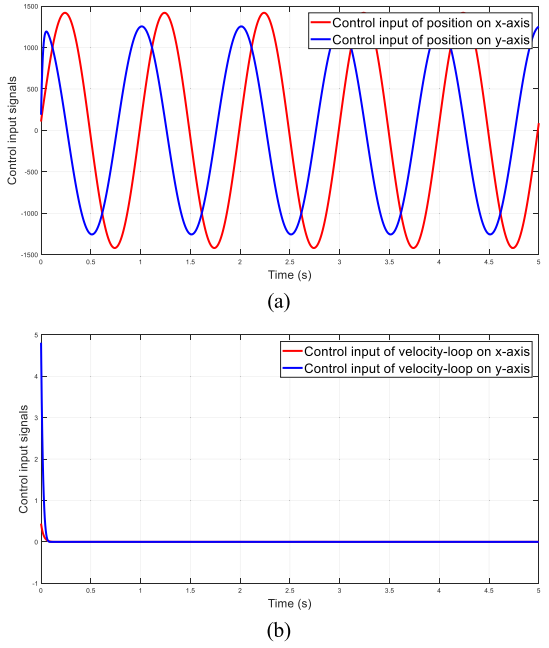

FIGURE 8. Control input signals: (a) control input of the position on the *x*- and y-axes and (b) control input of the velocity on the *x*- and y-axes.

$m_2 = 7, n_2 = 5, \eta_3 = 20, \chi_3 = 15, p_3 = 3, q_3 = 4, m_3 = 5, n_3 = 4, \eta_4 = 30, \chi_4 = 20, p_4 = 7, q_4 = 8, m_4 = 3,$ and $n_4 = 2$. The performances of control input and severe disturbance observer are better these values in case 1. These values are as follows:

With the small gains of fixed-time control, chattering will be suppressed. However, the response will last longer than that case of high gains control. The estimated disturbances are as follows:

The sine functions of $d_x = 20.\sin(2\pi t)$ and $d_y = 15.\sin(2\pi t)$ were tested on the *x*- and *y*-axes for case 2. In the comparison of the two cases, the sine function was estimated more easily because the original point of the sine functions and the disturbance observer are identical. For the cosine function, the oscillation will occur for the estimated disturbance in response to the tested disturbance. The oscillation of the estimated disturbance is realistic. To show the

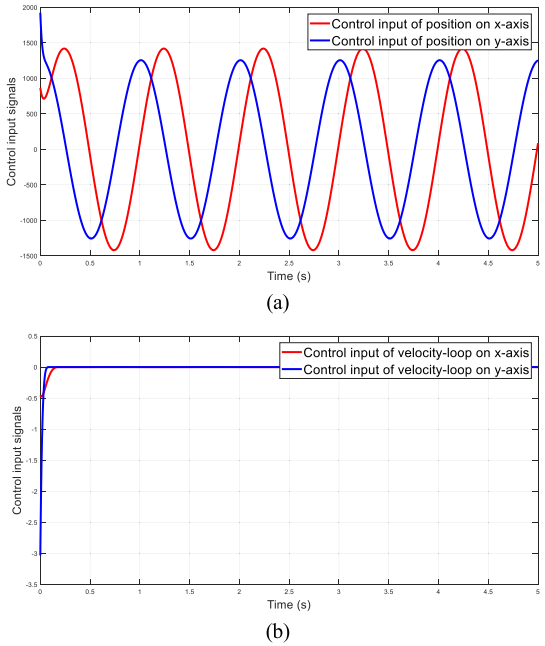

FIGURE 9. Control input signals: (a) control input of the position on the *x*- and y-axes and (b) control input of the velocity on the *x*- and y-axes.

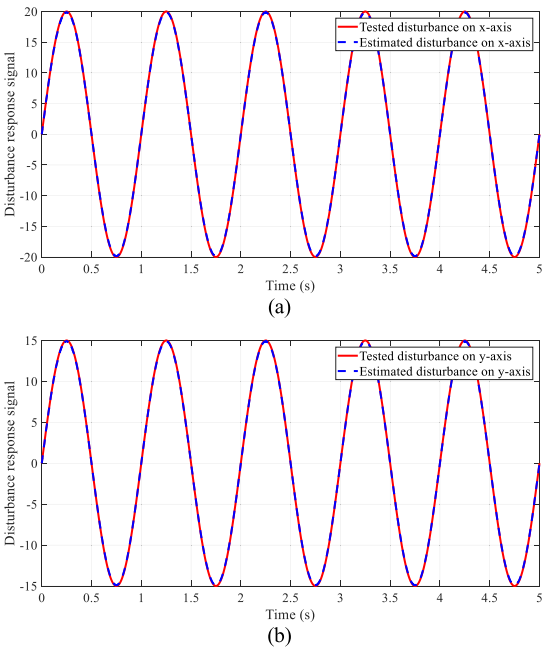

FIGURE 10. Tested and estimated disturbances on the *x*-axis (a) and *y*-axes (b).

independence of the tracking error on the initial states, this case tested the initial on x- and y-axes are ten times in compare with these initial in the first case. The tracking errors are shown as follows:

The settling times on the position of the x-axis and y-axis are $T_{e1} < 0.17$ seconds and $T_{e2} < 0.1$ seconds, respectively. The settling times on the velocity of the x-axis and y-axis are $T_{e3} < 0.151$ seconds and $T_{e4} \sim 0$ second, respectively.

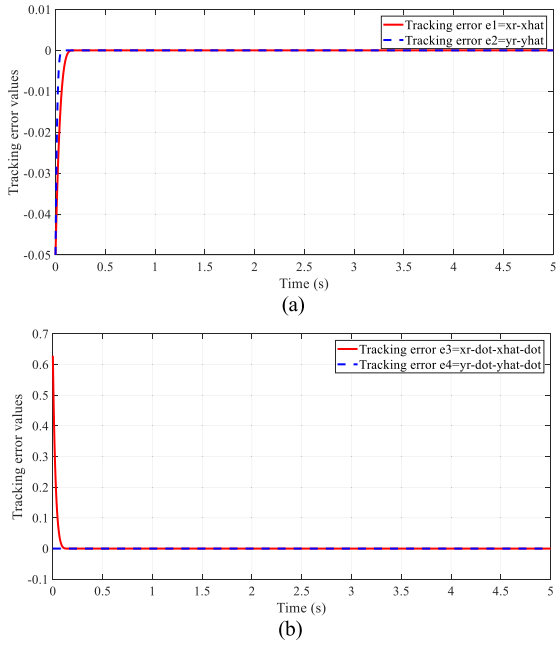

FIGURE 11. Tracking errors of position (a) and velocity (b).

These values are used to confirm that the tracking error values are weaken dependence on the initial states.

V. CONCLUSION

This paper modeled a nonlinear MEMS in the T-S fuzzy model, and this is an important step for the design of the robust control techniques for MEMS gyroscope systems. Furthermore, a new exogenous disturbance observer based on the FTSMC for a MEMS gyroscope system was investigated with exponentially convergent speed. The novelties of this study are the design of the sliding mode control by the reference and estimated states and the disturbance was simple and effective disturbance observer via the tracking error values of the measured and estimated states. The tracking error values are very small, and without overshoots, and the settling times are very short. A MATLAB simulation was used to verify that the proposed control theories are correct and powerful for T-S fuzzy MEMS gyroscopes. In the near future, the fixed-disturbance based on robust control of a T-S MEMS gyroscope will be considered to improve the performance of MEMS control systems. The direction of a new state observer and new state feedback control will also be considered.

REFERENCES

[1] M. Hosseini-Pishrobat and J. Keighobadi, "Robust output regulation of a triaxial MEMS gyroscope via nonlinear active disturbance rejection," *Int. J. Robust Nonlinear Control*, vol. 28, no. 5, pp. 1830–1851, Mar. 2018.
[2] M. Rahmani, "MEMS gyroscope control using a novel compound robust control," *ISA Trans.*, vol. 72, pp. 37–43, Jan. 2017.
[3] D. Lei, T. Wang, D. Cao, and J. Fei, "Adaptive dynamic surface control of MEMS gyroscope sensor using fuzzy compensator," *IEEE Access*, vol. 4, pp. 4148–4154, Aug. 2016.
[4] D. Wu, D. Cao, T. Wang, Y. Fang, and J. Fei, "Adaptive neural LMI-based H-infinity control for MEMS gyroscope," *IEEE Access*, vol. 4, pp. 6624–6630, 2016.

[5] Y. Chu, J. Fei, and S. Hou, "Adaptive neural backstepping PID global sliding mode fuzzy control of MEMS gyroscope," *IEEE Access*, vol. 7, pp. 37918–37926, 2019.
[6] J. Fei and Z. Feng, "Fractional-order finite-time super-twisting sliding mode control of micro gyroscope based on double-loop fuzzy neural network," *IEEE Trans. Syst., Man, Cybern. Syst.*, early access, Mar. 25, 2020, doi: 10.1109/TSMC.2020.2979979.
[7] J. Fei and Z. Wang, "Multi-loop recurrent neural network fractional-order terminal sliding mode control of MEMS gyroscope," *IEEE Access*, vol. 8, pp. 167965–167974, 2020, doi: 10.1109/ACCESS.2020.3022675.
[8] H. Wang, L. Hua, Y. Guo, and C. Lu, "Control of Z-axis MEMS gyroscope using adaptive fractional order dynamic sliding mode approach," *IEEE Access*, vol. 7, pp. 133008–133016, 2019.
[9] R. Zhang, T. Shao, W. Zhao, A. Li, and B. Xu, "Sliding mode control of MEMS gyroscopes using composite learning," *Neurocomputing*, vol. 275, pp. 2555–2564, Jan. 2018.
[10] R. Zhang, B. Xu, and P. Shi, "Output feedback control of micromechanical gyroscopes using neural networks and disturbance observer," *IEEE Trans. Neural Netw. Learn. Syst.*, early access, Oct. 29, 2020, doi: 10.1109/TNNLS.2020.3030712.
[11] Y. Fang, S. Wang, J. Fei, and M. Hua, "Adaptive control of MEMS gyroscope based on T–S fuzzy model," *Discrete Dyn. Nature Soc.*, vol. 2015, Feb. 2015, Art. no. 419643.
[12] S. Wang and J. Fei, "Robust adaptive sliding mode control of MEMS gyroscope using T–S fuzzy model," *Nonlinear Dyn.*, vol. 77, nos. 1–2, pp. 361–371, Jul. 2014.
[13] T. Takagi and M. Sugeno, "Fuzzy identification of systems and its applications to modeling and control," *IEEE Trans. Syst., Man, Cybern.*, vol. SMC-15, no. 1, pp. 116–132, Jan. 1985.
[14] K. Tanaka and H. Wang, *Fuzzy Control Systems Design and Analysis: A Linear Matrix Inequality Approach*. New York, NY, USA: Wiley, 2001.
[15] V.-P. Vu, W.-J. Wang, H.-C. Chen, and J. M. Zurada, "Unknown input-based observer synthesis for a polynomial T–S fuzzy model system with uncertainties," *IEEE Trans. Fuzzy Syst.*, vol. 26, no. 3, pp. 1447–1458, Jun. 2018.
[16] R. Sakthivel, K. Raajananthini, O. M. Kwon, and S. Mohanapriya, "Estimation and disturbance rejection performance for fractional order fuzzy systems," *ISA Trans.*, vol. 92, pp. 65–74, Sep. 2019.
[17] V.-N. Giap, S.-C. Huang, Q. D. Nguyen, and T.-J. Su, "Robust control-based disturbance observer and optimal states feedback for T–S fuzzy systems," *J. Low Freq. Noise, Vib. Act. Control*, pp. 1–17, Dec. 2020, doi: 10.1177/1461348420981181.
[18] R. Sakthivel, S. Harshavarthini, R. Kavikumar, and Y.-K. Ma, "Robust tracking control for fuzzy Markovian jump systems with time-varying delay and disturbances," *IEEE Access*, vol. 6, pp. 66861–66869, 2018.
[19] P. Selvaraj, R. Sakthivel, and H. Reza Karimi, "Equivalent-input-disturbance-based repetitive tracking control for Takagi–Sugeno fuzzy systems with saturating actuator," *IET Control Theory Appl.*, vol. 10, no. 15, pp. 1916–1927, Oct. 2016.
[20] V. N. Giap, Q. D. Nguyen, and S. C. Huang, "Synthetic adaptive fuzzy disturbance observer and sliding-mode control for chaos-based secure communication systems," *IEEE Access*, vol. 9, pp. 23907–23928, 2021.
[21] R. Sakthivel, R. Sakthivel, O. Kwon, and P. Selvaraj, "Synchronisation of stochastic T–S fuzzy multi-weighted complex dynamical networks with actuator fault and input saturation," *IET Control Theory Appl.*, vol. 14, no. 14, pp. 1957–1967, Sep. 2020.
[22] V. N. Giap, S.-C. Huang, Q. D. Nguyen, and T.-J. Su, "Disturbance observer-based linear matrix inequality for the synchronization of Takagi–Sugeno fuzzy chaotic systems," *IEEE Access*, vol. 8, pp. 225805–225821, Dec. 2020.
[23] M. Chilali, P. Gahinet, and P. Apkarian, "Robust pole placement in LMI regions," *IEEE Trans. Autom. Control*, vol. 44, no. 12, pp. 2257–2270, Dec. 1999.
[24] C. Mahmoud and G. Pascal, "H_∞ design with pole placement constraints: An LMI capproach," *IEEE Trans. Autom. Control*, vol. 41, no. 3, pp. 358–367, Mar. 1996.
[25] V. Utkin, "Variable structure systems with sliding modes," *IEEE Trans. Autom. Control*, vol. AC-22, no. 2, pp. 212–222, Apr. 1977.
[26] C. C. Fuh, "Variable-thickness boundary layers for sliding mode contro," *J. Mar. Sci. Tech.*, vol. 16, no. 4, pp. 288–294, Dec. 2008.
[27] V.-N. Giap and S.-C. Huang, "Effectiveness of fuzzy sliding mode control boundary layer based on uncertainty and disturbance compensator on suspension active magnetic bearing system," *Meas. Control*, vol. 53, nos. 5–6, pp. 934–942, Mar. 2020.
[28] G. Gandikota and D. K. Das, "Disturbance observer–based adaptive boundary layer sliding mode controller for a type of nonlinear multiple-input multiple-output system," *Int. J. Robust Nonlinear Control*, vol. 29, no. 17, pp. 5886–5912, Aug. 2019.
[29] A. S. S. Abadi, P. A. Hosseinabadi, N. B. Soin, and S. Mekhilef, "Chattering-free adaptive finite-time sliding mode control for trajectory tracking of MEMS gyroscope," *Autom. Control Comput. Sci.*, vol. 54, no. 4, pp. 335–345, Sep. 2020.
[30] A. S. S. Abadi, P. A. Hosseinabadi, and S. Mekhilef, "Fuzzy adaptive fixed-time sliding mode control with state observer for a class of high-order mismatched uncertain systems," *Int. J. Control, Autom. Syst.*, vol. 18, no. 10, pp. 2492–2508, May 2020.
[31] A. Polyakov, "Nonlinear feedback design for fixed-time stabilization of linear control systems," *IEEE Trans. Autom. Control*, vol. 57, no. 8, pp. 2106–2110, Aug. 2012.
[32] Y. Tian, Y. Cai, and Y. Deng, "A fast nonsingular terminal sliding mode control method for nonlinear systems with fixed-time stability guarantees," *IEEE Access*, vol. 8, pp. 60444–60454, 2020.
[33] Y. Liu, F. Zhang, P. Huang, and Y. Lu, "Fixed-time consensus tracking for second-order multiagent systems under disturbance," *IEEE Trans. Syst., Man, Cybern. Syst.*, early access, Oct. 15, 2019, doi: 10.1109/TSMC.2019.2944392.
[34] S. Wu, X. Su, and K. Wang, "Time-dependent global nonsingular fixed-time terminal sliding mode control-based speed tracking of permanent magnet synchronous motor," *IEEE Access*, vol. 8, pp. 186408–186420, Oct. 2020.
[35] K. A. Langueh, G. Zheng, and T. Floquet, "Fixed-time sliding mode-based observer for non-linear systems with unknown parameters and unknown inputs," *IET Control Theory Appl.*, vol. 14, no. 14, pp. 1920–1927. Sep. 2020.
[36] S. Shi, J. Gu, S. Xu, and H. Min, "Globally fixed-time high-order sliding mode control for new sliding mode systems subject to mismatched terms and its application," *IEEE Trans. Ind. Electron.*, vol. 67, no. 12, pp. 10776–10786, Dec. 2020.
[37] W.-H. Chen, "Disturbance observer based control for nonlinear systems," *IEEE/ASME Trans. Mechatronics*, vol. 9, no. 4, pp. 706–710, Dec. 2004.
[38] A. T. Nguyen, B. A. Basit, H. H. Choi, and J.-W. Jung, "Disturbance attenuation for surface-mounted PMSM drives using nonlinear disturbance observer-based sliding mode control," *IEEE Access*, vol. 8, pp. 86345–86356, May 2020.
[39] J. Huang, S. Ri, L. Liu, Y. Wang, J. Kim, and G. Pak, "Nonlinear disturbance observer-based dynamic surface control of mobile wheeled inverted pendulum," *IEEE Trans. Control Syst. Technol.*, vol. 23, no. 6, pp. 2400–2407, Nov. 2015.
[40] J. Fei, H. Wang, and Y. Fang, "Novel neural network fractional-order sliding-mode control with application to active power filter," *IEEE Trans. Syst., Man, Cybern. Syst.*, early access, Apr. 15, 2021, doi: 10.1109/TSMC.2021.3071360.
[41] J. Fei, Z. Wang, X. Liang, Z. Feng, and Y. Xue, "Fractional sliding mode control for micro gyroscope based on multilayer recurrent fuzzy neural network," *IEEE Trans. Fuzzy Syst.*, early access, Mar. 9, 2021, doi: 10.1109/TFUZZ.2021.3064704.
[42] J. Fei, Y. Chen, L. Liu, and Y. Fang, "Fuzzy multiple hidden layer recurrent neural control of nonlinear system using terminal sliding-mode controller," *IEEE Trans. Cybern.*, early access, Mar. 12, 2021, doi: 10.1109/TCYB.2021.3052234.
[43] X. Shao, L. Xu, and W. Zhang, "Quantized control capable of appointed-time performances for quadrotor attitude tracking: Experimental validation," *IEEE Trans. Ind. Electron.*, early access, May 18, 2021, doi: 10.1109/TIE.2021.3079887.
[44] S. Hwang and H. S. Kim, "Extended disturbance observer-based integral sliding mode control for nonlinear system via T–S fuzzy model," *IEEE Access*, vol. 8, pp. 116090–116105, Jun. 2020.
[45] S. Hwang, J. B. Park, and Y. H. Joo, "Disturbance observer-based integral fuzzy sliding-mode control and its application to wind turbine system," *IET Control Theory Appl.*, vol. 13, no. 12, pp. 1891–1900, Aug. 2019.
[46] X. Liu and D. Liu, "Composite control of nonlinear robotic system with exogenous disturbance," *IEEE Access*, vol. 7, pp. 19564–19571, 2019.
[47] H. G. Zhang, J. Han, Y. Wang, and C. M. Luo, "Fault-tolerant control of a nonlinear system based on generalized fuzzy hyperbolic model and adaptive disturbance observer," *IEEE Trans. Syst., Man, Cybern., Syst.*, vol. 47, no. 8, pp. 2289–2300, Aug. 2017.

[48] M. Rahmani, M. H. Rahman, and M. Nosonovsky, "A new hybrid robust control of MEMS gyroscope," *Microsyst. Technol.*, vol. 26, no. 3, pp. 853–860, Mar. 2020.
[49] X. Shao, Y. Shi, W. Zhang, and H. Cao, "Neurodynamic approximation-based quantized control with improved transient performances for micro-electromechanical system gyroscopes: Theory and experimental results," *IEEE Trans. Ind. Electron.*, vol. 68, no. 10, pp. 9972–9983, Oct. 2021, doi: 10.1109/TIE.2020.3026297.
[50] X. Shao, Z. Cao, and H. Si, "Neurodynamic formation maneuvering control with modified prescribed performances for networked uncertain quadrotors," *IEEE Syst. J.*, early access, Oct. 22, 2020, doi: 10.1109/JSYST.2020.3022901.
[51] X. Shao, Y. Shi, W. Zhang, and J. Zhao, "Prescribed fast tracking control for flexible air-breathing hypersonic vehicles: An event-triggered case," *Chin. J. Aeronaut.*, Apr. 2021, doi: 10.1016/j.cja.2021.03.019.
[52] X. Shao, Y. Shi, and W. Zhang, "Fault-tolerant quantized control for flexible air-breathing hypersonic vehicles with appointed-time tracking performances," *IEEE Trans. Aerosp. Electron. Syst.*, vol. 57, no. 2, pp. 1261–1273, Apr. 2021, doi: 10.1109/TAES.2020.3040519.
[53] X. Shao, B. Tian, and W. Yang, "Fixed-time trajectory following for quadrotors via output feedback," *ISA Trans.*, vol. 110, pp. 213–224, Apr. 2021.
[54] B. Xu, R. Zhang, S. Li, W. He, and Z. Shi, "Composite neural learning-based nonsingular terminal sliding mode control of MEMS gyroscopes," *IEEE Trans. Neural Netw. Learn. Syst.*, vol. 31, no. 4, pp. 1375–1386, Apr. 2020.
[55] X. Shao and Y. Shi, "Neural adaptive control for MEMS gyroscope with full-state constraints and quantized input," *IEEE Trans. Ind. Informat.*, vol. 16, no. 10, pp. 6444–6454, Oct. 2020, doi: 10.1109/TII.2020.2968345.
[56] H. Si, X. Shao, and W. Zhang, "MLP-based neural guaranteed performance control for MEMS gyroscope with logarithmic quantizer," *IEEE Access*, vol. 8, pp. 38596–38605, 2020.
[57] Y. Shi, X. Shao, W. Yang, and W. Zhang, "Event-triggered output feedback control for MEMS gyroscope with prescribed performance," *IEEE Access*, vol. 8, pp. 26293–26303, 2020, doi: 10.1109/ACCESS.2020.2971018.
[58] B. Vaseghi, M. A. Pourmina, and S. Mobayen, "Finite-time chaos synchronization and its application in wireless sensor networks," *Trans. Inst. Meas. Control*, vol. 40, no. 13, pp. 3788–3799, Nov. 2017.
[59] S. Hashemi, M. A. Pourmina, S. Mobayen, and M. R. Alagheband, "Design of a secure communication system between base transmitter station and mobile equipment based on finite-time chaos synchronisation," *Int. J. Syst. Sci.*, vol. 51, no. 11, pp. 1969–1986, Aug. 2020.
[60] S. Mobayen, J. Ma, G. Pujol-Vazquez, L. Acho, and Q. Zhu, "Adaptive finite-time stabilization of chaotic flow with a single unstable node using a nonlinear function-based global sliding mode," *Iranian J. Sci. Technol., Trans. Electr. Eng.*, vol. 43, no. S1, pp. 339–347, Jul. 2019.
[61] B. Vaseghi, S. Mobayen, S. S. Hashemi, and A. Fekih, "Fast reaching finite time synchronization approach for chaotic systems with application in medical image encryption," *IEEE Access*, vol. 9, pp. 25911–25925, 2021, doi: 10.1109/ACCESS.2021.3056037.
[62] X. Shao and Y. Shi, "Neural-network-based constrained output-feedback control for MEMS gyroscopes considering scarce transmission bandwidth," *IEEE Trans. Cybern.*, early access, May 25, 2021, doi: 10.1109/TCYB.2021.3070137.

VAN NAM GIAP received the B.S. degree in control engineering and automation from the Hanoi University of Science and Technology, Hanoi, Vietnam, in 2015, and the master's degree in electronic engineering from the National Kaohsiung University of Applied and Sciences, Kaohsiung, Taiwan, in 2017. He is currently pursuing the Ph.D. degree in mechanical engineering with the National Kaohsiung University of Science and Technology, Taiwan. His research interests include sliding mode control, disturbance and uncertainty estimation, fuzzy logic control, secure communication, and the magnetic bearing systems and its applications.

HONG-SON VU received the B.S. degree in electrical engineering from the Hung Yen University of Technology and Education, Hung Yen, Vietnam, in 2008, the M.S. degree in automation engineering from Military Technical Academy, Hanoi, Vietnam, in 2011, and the Ph.D. degree from Feng Chia University, Taichung, Taiwan, in June 2016.

Since 2008, he has been with the Faculty of Electrical and Electronic Engineering, Hung Yen University of Technology and Education, as a Lecturer. He has published more than 17 refereed papers/articles in low-power VLSI architecture designs for visual/audio signal processing. His research interests include VLSI architecture design, system-on-chip design, object detection, electronic circuits, and active noise cancellation.

Dr. Vu was a recipient of the Excellent Award of MXIC Design Contest, Taiwan, in 2014.

QUANG DICH NGUYEN received the B.S. degree in electrical engineering from the Hanoi University of Technology, Hanoi, Vietnam, in 1997, the M.S. degree in electrical engineering from the Dresden University of Technology, Dresden, Germany, and the Ph.D. degree from Ritsumeikan University, Kusatsu, Japan, in 2003 and 2010, respectively. Since 2000, he has been with the Hanoi University of Science and Technology, where he is currently an Associate Professor, and the Executive Dean of the Institute for Control Engineering and Automation. His research interests include magnetic bearings, self-bearing motors, and sensorless motor control.

SHYH-CHOUR HUANG (Senior Member, IEEE) received the bachelor's degree in aeronautics and astronautics engineering from the National Cheng Kung University, Taiwan, in 1980, and the Ph.D. degree in mechanical engineering from the University of Cincinnati, USA, in 1990. He is currently a Professor of mechanical engineering with the National Kaohsiung University of Science and Technology, Taiwan. His research interests include micro-electromechanical systems' design, biomechanics, compliant mechanisms, multibody dynamics, fuzzy logic control, vibration control, and optimization algorithms.